

## ELASTO-KINEMATIC MODEL OF SUSPENSION WITH FLEXIBLE SUPPORTING ELEMENTS

TOMÁŠ VRÁNA<sup>a,\*</sup>, JOSEF BRADÁČ<sup>b</sup>, JAN KOVANDA<sup>c</sup>

<sup>a</sup> Department of Vehicles and Ground Transport, Faculty of Engineering, CULS Prague, Kamýcká 129, 165 21 Praha – Suchbátka, Czech Republic

<sup>b</sup> Department of Automotive Technology, Škoda Auto University, Na Karmeli 1457, 293 60 Mladá Boleslav, Czech Republic

<sup>c</sup> Department of Security Technologies and Engineering, Faculty of Transportation Sciences, CTU in Prague, Konviktská 20, 110 00 Praha 1, Czech Republic

\* corresponding author: [vrana.ds@seznam.cz](mailto:vrana.ds@seznam.cz)

**ABSTRACT.** This paper analyzes the impact of flexibility of individual supporting elements of independent suspension on its elasto-kinematic characteristics. The toe and camber angle are the geometric parameters of the suspension, which waveforms and their changes under the action of vertical, longitudinal and transverse forces affect the stability of the vehicle. To study these dependencies, the computational multibody system (MBS) model of axle suspension in the system HyperWorks is created. There are implemented Finite-Element-Method (FEM) models reflecting the flexibility of the main supporting elements. These are subframe, the longitudinal arms, transverse arms and knuckle. Flexible models are developed using Component Mode Synthesis (CMS) by Craig-Bampton. The model further comprises force elements, such as helical springs, shock absorbers with a stop of the wheel and the anti-roll bar. Rubber-metal bushings are modeled flexibly, using nonlinear deformation characteristics. Simulation results are validated by experimental measurements of geometric parameters of real suspension.

**KEYWORDS:** independent suspension, MBS model, flexible model of supporting elements, wheel toe, wheel camber, HyperWorks.

### 1. INTRODUCTION

Nowadays, vehicles are equipped with powerful power units and achieve very high speeds. At the same time, the number of vehicles is significantly increasing and causes high traffic density on the roads and thus increases the number of accidents and traffic safety problem. It is important to study not only passive safety (reducing the consequences of road traffic accidents), but mainly active safety, which aims to prevent traffic accidents. This technical discipline is closely related to the vehicle dynamics. The mathematical description of vehicle behavior is possible to find in publications [1, 2], which generally show the importance of the topic. Specifically, publication [3] deals with the creating of the MBS computational model of the whole vehicle using non-linear FEM model of the tire, which is then used for simulations and research of vehicle behavior on rough road surfaces. Driving characteristics and vehicle behavior are affected by many aspects. One of the main aspects is elasto-kinematic characteristic of the suspension during different loading modes. High attention should be paid not only to the investigation of the vehicle behavior, but also to the field of suspension elasto-kinematics. It is important to deal with the study and preparation of computational models of suspension and increase their accuracy and efficiency. The term elasto-kinematic characteristics

of the suspension is defined as the change of geometrical parameters of the suspension (toe angle, camber angle) due to the action of the wheel load in vertical, longitudinal and transverse direction of the vehicle. For the study of kinematic characteristics of the suspension mechanism, without considering flexibility, it is most effective to use methods of transformation matrices [4]. The most commonly used method is disconnected loop method or the method of removing the body, which leads to simpler mathematical solution thanks to the lower number of equations. Kinematic analysis and analysis of mechanism in case of McPherson suspension, wishbone and five-link suspension is shown in [5–7]. Influence of positioning of kinematic points on the camber and toe angle of independent multi-link suspension is shown in [8]. Computational model is created in HyperWorks system and includes the flexible model of longitudinal arm. Dependencies of geometrical parameters of the vertical movement of the wheels are provided for the movement of kinematic points in the vertical and transverse direction by the value of  $\pm 1$  and  $\pm 2$  mm. Sensitivity analysis of elasto-kinematic and dynamic properties on the deformation characteristics of bushings and supporting elements for independent suspension McPherson is shown in [9]. The MBS computational model, taking into account the flexibility of rubber-metal bushings, was created in the MSC.ADAMS/Car system. The

flexibility of supporting elements was not taken into account in this model. Another work [10] proposes and explores verification method to validate the results of simulations elasto-kinematic characteristics of the front axle McPherson suspension. In [11], there is presented the concept of a new mechanism of independent axle suspension, which was created during optimizing the shape of the contact surface of the tire-road. Suspension kinematics is described by equations for closed loop mechanism, solved using the determinant of Sylvester matrix. MBS models that take into account the flexibility of supporting elements of the suspension are not used in the automotive industry because of their intensity and complexity in preparing thus the knowledge of how their flexibility affects the elasto-kinematics of suspension is missing. The aim of this paper is to show and describe the effect of flexibility of supporting components of independent suspension on its elasto-kinematic properties in defined loading modes. To achieve this goal, several variants of the computational models of an independent rear suspension, which reflecting the deformation characteristics of rubber-metal bushings and flexibility of suspension parts such as subframe, longitudinal and transverse arms and knuckle were used. The simulations clearly show the influence of flexibility of individual supporting elements on elasto-kinematic behaviour of suspension that is described by the toe angle  $\delta$  and the camber angle  $\gamma$  at defined load. The results compared with the model containing absolutely rigid supporting elements are validated by experimental measurements. The presented computational model was created in several modules of Altair HyperWorks system [12].

## 2. MBS MODEL IN HYPERWORKS

Multi body system (MBS) model is a mechanical coupled system, which consists mostly of absolutely rigid bodies, but may also contain FEM models that can have flexible behaviour. All the elements are connected by linkages, which may be kinematic and elasto-kinematic with the flexible description. According to the kinematic structure, it is possible to determine the number of degrees of freedom of  $DOF$  system using equation

$$DOF = 6(NU - 1) - 5(RO + SL) - 3SP, \quad (1)$$

where  $NU$  is the number of elements of suspension mechanism including frame,  $RO$  is the number of rotational kinematic pairs (KP),  $SL$  is the number of translation kinematic pairs KP and  $SP$  is the number of spherical KP.

Mechanical system of elements is described by the dependent coordinate  $q_i$ , number  $N > DOF$  arranged into a vector of dependent coordinate  $\mathbf{q}$  according to (2)

$$\mathbf{q} = [q_1, q_2, \dots, q_i, \dots, q_N]^T. \quad (2)$$

Mathematical solver MotionSolve of HyperWorks system assembles the equations of motion for the mechanical system, created in the MBS model of pre-processor MotionView, by help of the Lagrange equations [13, 14] of mixed type written in the matrix form (3),

$$\frac{d}{dt} \left( \frac{\partial E}{\partial \dot{\mathbf{q}}} \right) - \frac{\partial E}{\partial \mathbf{q}} = \mathbf{Q} + \frac{\partial \mathbf{f}^T}{\partial \mathbf{q}} \boldsymbol{\lambda}, \quad (3)$$

where  $E$  is the kinetic energy of the mechanical system, the vector of generalized forces  $\mathbf{Q} = [Q_1, Q_2, \dots, Q_i, \dots, Q_N]^T$ , the vector of holonomic binding conditions  $\mathbf{f} = [f_1, f_2, \dots, f_k, \dots, f_R]^T$  and the vector of Lagrange multipliers  $\boldsymbol{\lambda} = [\lambda_1, \lambda_2, \dots, \lambda_k, \dots, \lambda_R]^T$ . The number of Lagrange equations in the matrix form (3) is then  $DOF + R$ , where  $R = N - DOF$ .

Lagrange equations (3) must be supplemented by coupling conditions that can be written in matrix equation (4)

$$\mathbf{f}(\mathbf{q}) = \begin{bmatrix} f_1(\mathbf{q}) \\ f_2(\mathbf{q}) \\ \vdots \\ f_k(\mathbf{q}) \\ \vdots \\ f_R(\mathbf{q}) \end{bmatrix} = \begin{bmatrix} 0 \\ 0 \\ \vdots \\ 0 \\ \vdots \\ 0 \end{bmatrix} = 0. \quad (4)$$

These coupling conditions, in the total number of  $R$ , represent a geometric definition of kinematic pairs connecting the body system [14].

The system of differential-algebraic equations formed by Lagrange equations (3) and coupling conditions (4) is solved in mathematical tool MotionSolve by numerical mathematics. Unknown vector of dependent coordinate  $\mathbf{q}$  in the individual iteration steps is found by DAE – integrator, which is designated as HyperWorks DSTIFF [15].

## 3. MBS COMPUTATIONAL MODEL OF INDEPENDENT SUSPENSION

Examined MBS model of independent suspension was created in the pre-processor MotionView of HyperWorks system. The complex computational model was created by inserting flexible FEM models into the MBS model, see Figure 1.

### 3.1. CREATION OF MBS MODEL

Special type of suspension was chosen for the model. It is kinematical determined mechanism according to the diagram in Figure 2.

This means that for the kinematic functionality ( $DOF = 1$ ) the certain defined flexibility of longitudinal arms 2, which have to deform in the longitudinal direction during the vertical motion of the wheel (wheel centre – point WC), is required. When the calculation model contains the description of absolutely rigid longitudinal arm 2, this arm must be connected to

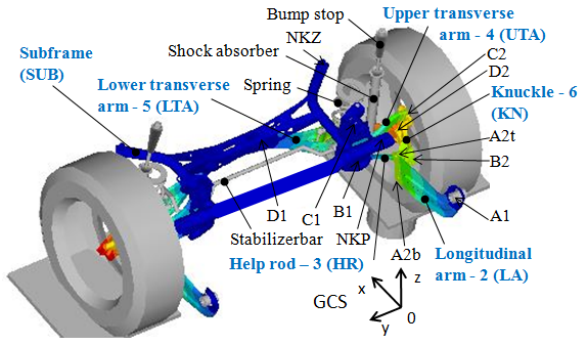


FIGURE 1. Computational MBS model with implemented FEM flexible models of supporting elements.

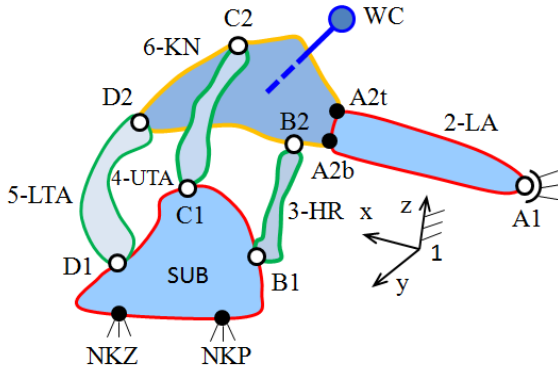


FIGURE 2. Computational MBS model with implemented FEM flexible models of supporting elements.

the knuckle 6 via a rotary coupling to fulfil  $DOF = 1$ . Elast-Flex LA model was created as the basic model with flexible longitudinal arms (LA), which have to be joined to the knuckle via the FIX links to correspond to the real suspension. Other flexible bodies were implemented into the models, such as the upper transverse arm (UTA), the lower transverse arm (LTA), the help rod (HR), knuckle (KN) and the subframe (SUB). Thus the complex elasto-kinematic model Elast+Flex All, containing the description of all the supporting elements and other flexible bodies, was created. For example, it is the model Elast+Flex LA+Flex SUB (flexible rubber-metal bushings, flexible longitudinal arms and subframe) or Elast+Flex LA+Flex LTA (flexible bushings, longitudinal arms and lower transverse arms). The model Elast+Rigid (flexible bushings, supporting elements absolutely rigid) was also created. It is used for the comparison with models comprising flexible bodies.

The position of suspension mechanism was defined in MotionView by Cartesian coordinates of kinematic points (Table 1). These data were obtained from measurements on the real vehicle. Because of the symmetry of the model around the  $x$  axis in CGS only the left side of the model is displayed.

The MBS model includes also elastic elements (helical spring with linear stiffness of 30 N/mm and torsion stabilizer, shock absorber and bumper) that affect the

Kinematic point	Type KP	Coordinate in GCS		
		$x$ [mm]	$y$ [mm]	$z$ [mm]
A1	BALL	2098	-603	36
A2t	FIX	2402	-595	27
A2b	FIX	2402	-595	-33
B1	BALL	2480	-365	-21
B2	BALL	2502	-678	-40
C1	BALL	2534	-380	143
C2	BALL	2540	-685	130
D1	BALL	2805	-105	-10
D2	BALL	2790	-685	-45
NKP	FIX	2410	-482	72
NKZ	FIX	2860	-485	95

TABLE 1. Type and position of KP global coordinate system (GCS).

rubber-metal bushings properties and influence the elasto-kinematic behaviour of suspension. Deformation properties of rubber-metal bushings are described in the same way for all variants of the model and thus by means of a force-deformation dependence. All characteristics for each bushing were experimentally measured for six load cases. Figure 3 shows the composition and method of measuring the load to determine the radial deformation characteristics  $D_x = f(F_x)$  A1-bushing.

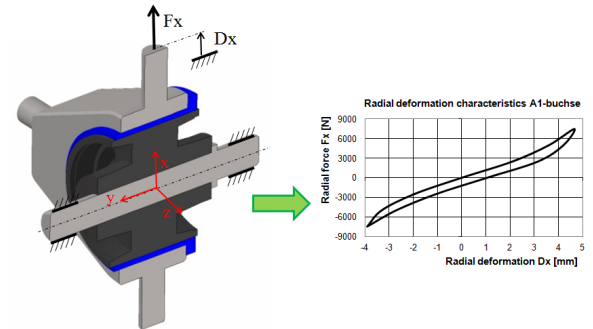


FIGURE 3. Measurement of deformation characteristics  $D_x = f(F_x)$  of rubber-metal bushing.

### 3.2. FLEXIBLE MODELS OF SUSPENSION SUPPORTING ELEMENTS

Flexible models of the supporting elements of the suspension are generated by Component Mode Synthesis (CMS), which is processed in the tool FLEXPREP in MotionView. CMS transfers the body from node to modal representation that characterizes its flexible behaviour using natural frequencies and natural shapes. Craig-Bampton method [12, 16] was chosen as the CMS method that uses the linear combination of modal shapes  $\Phi$  and vector of modal coordinates  $s$  and approximates the vector of linear displacement  $dn$  of FEM network according to (5)

$$dn = \Phi \cdot s. \quad (5)$$

During the creation of flexible models of supporting elements the 3D CAD models in the module Hypermesh with precise geometry were created. They were subsequently discretized in Hypermesh module by finite element method. Figure 4 shows the FEM model of help rod (HR).

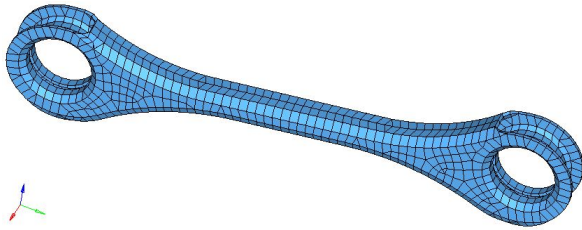


FIGURE 4. FEM model of help rod (HR).

The network was created on the base of combination of triangular and quadrangular elements. Surface network with PSHELL elements and assigned thickness was used for arms and the subframe. For discretization of knuckle volume, the network elements type PSOLID were used. The size of elements was chosen to be 5 mm. The number of elements and nodes of the network and their thicknesses for analyzed flexible elements are shown in Table 2. The total number of elements for all models of supporting elements is 136 103.

Element	No. of nodes [-]	No. of elements [-]	Thickness [mm]
SUB	24 238	24 309	3.5
LA	744	698	3
LTA	6 300	6 118	2.5
UTA	2 526	2 498	3.5
HR	1 211	1 103	3.0
KN	11 692	45 480	

TABLE 2. Number of elements and nodes for flexible supporting elements.

Knuckle material is cast iron with modulus of elasticity  $E = 1.76 \times 10^5$  MPa and the Poisson number  $\mu = 0.275$ . For subframe and arms it is steel with  $E = 2.10 \times 10^5$  MPa and  $\mu = 0.3$ .

The first three calculated natural shapes for the help rod (HR) are shown in Figure 5.

The value of the first natural frequency corresponding to the first shape is 390 Hz, the second natural frequency is 683 Hz and the third is 923 Hz. The natural frequency of other supporting elements is shown in Figure 6. The lowest natural frequency is for subframe (SUB), while the highest value is for knuckle (KN).

Created models with flexible elements were implemented to the MBS model. Output File of FEM models of supporting elements exported from Hypermesh has an extension .fem and enters the tool FLEX-PREP together with the definition of RBE2 Spider. The output is then the final flexible model in H3d format.

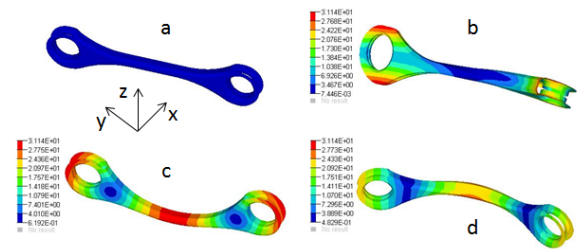


FIGURE 5. First three calculated natural shapes for the help rod (HR), a) undeformed state, b) first modal shape (torsion), c) second modal shape (bend around x axis), d) third modal shape (bend around z axis).

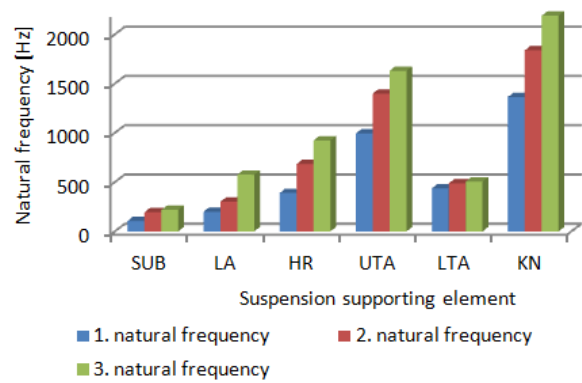


FIGURE 6. Comparison of first three natural frequencies [Hz] analyzed supporting elements.

### 3.3. CREATION OF INTERFACE NODES

Before inserting flexible FEM models into MBS model, the reference nodes, so-called RBE2-Spiders, were created. These help entities join the MBS kinematic model (Table 1) with the corresponding nodes of FEM simulation models of flexible supporting elements.

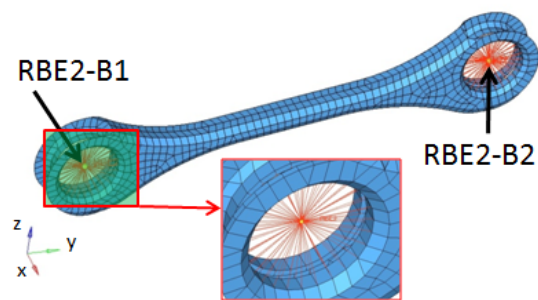


FIGURE 7. RBE2 spiders for help rod.

RBE2-Spiders for the help rod (HR) are shown in Figure 7. It is the point RBE2-B1, which joins the kinematic point B1 (the node No. 6 777) with 104 nodes of the inner arm housing at subframe. RBE2-B2 joins the kinematic point B2 (node 6 778) with 104 nodes of the knuckle housing. In the knuckle, there is also created inverse RBE2-B2, which joins the point B2 (node No. 31 061) with 134 nodes of knuckle hole

for housing the help rod (HR). Other RBE2-Spiders of other flexible bodies are created in a similar manner in Hypermesh module. The model of suspension thus contains 34 RBE2-Spiders.

#### 4. SIMULATIONS COMPUTATIONS

Elasto-kinematic properties of computational models were simulated using mathematical tool MotionSolve. For the calculations the time interval  $t = (0; 80)$  s and the time step  $\Delta t = 0.05$  s were set. The simulation model of wheel suspension was gradually loaded by three loading modes according to Figure 8.

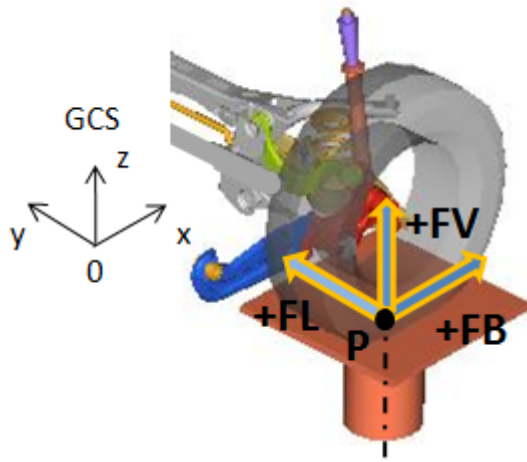


FIGURE 8. Definition of loading states for independent suspension.

In the first mode, the wheel support is loaded by vertical force  $FV$ , which causes a vertical movement of the wheels  $W_Z = \langle -105; 105 \rangle$  mm. Edge values  $\pm 105$  mm represent the upper and lower stop during the vertical movement of the wheel. In two other modes, the wheel support is loaded by side force that varies in the interval  $FL = \langle -10000; 10000 \rangle$  N and longitudinal braking force in the value  $FB = \langle 0; 10000 \rangle$  N. Furthermore, the static radius of the tire 286 mm, the radial stiffness 225 N/mm, for vehicle mass 1487 kg and a wheelbase of 2550 mm, were set up.

#### 5. VALIDATION OF MBS MODEL

Validation of computational model for the calculation of elasto-kinematic characteristics, taking into account the flexibility of supporting elements, was carried out at two levels. First moments of inertia calculated from models of deformable bodies in HyperWorks were compared with measured values of the moments of inertia of the real suspension elements. In the second step, the experimental measurement of geometrical parameters of the wheel suspension for validation of simulation results was prepared.

##### 5.1. VALIDATION OF INERTIA MOMENTS OF SUSPENSION SUPPORTING ELEMENTS

Moments of inertia of supporting elements calculated from geometrical models in Hypermesh have been verified by experimental measurements on so-called torsion hanger [9]. This measuring device (Figure 9) consists of a lightweight circular plate having a diameter  $d = 0.8$  m, hinged at points A, B, C using thin cords of length  $l = 3.5$  m. The suspension points are located at pitch circle of radius  $r = 0.375$  m.

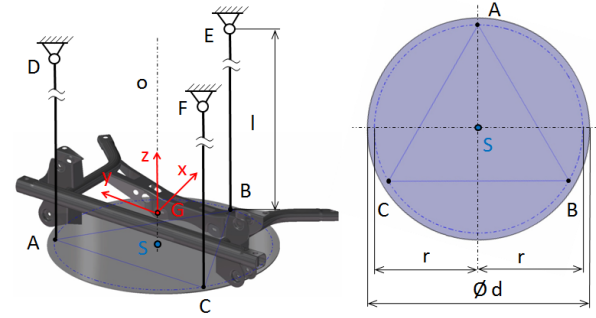


FIGURE 9. Measurement of inertia moment  $I_{zz}$  of subframe using torsion hanger.

The aim is to find moments of inertia about axes that are passing through the center of gravity, and are parallel to the axes of GCS. Using this definition, the moments of inertia are calculated in Hypermesh and transferred to MotionView. The measured body is mounted on a plate, with its center of gravity  $G$  placed above the center of the plate  $S$ , so that the axis of the rotation of the plate (in Figure 9 marked as  $o$ ) is identical with the axis to which the inertia is being found. When we are looking for the moment of inertia  $I_{zz}$ , then the subframe axis coincides with the suspension axis  $o$ . After the motion starts, the hanger oscillates torsionally and the time period  $T$  is measured by the help of stop watch. From the equality of kinetic and potential energy, the final relation (6) is found. This relation is used to calculate the moment of inertia  $J_2$  [kg m<sup>2</sup>] of the particular supporting element.

$$J_2 = \frac{(m_1 + m_2)gr^2T^2}{4\pi^2l} - J_1, \quad (6)$$

where  $m_1$  [kg] is the weight of the plate of torsion hanger,  $m_2$  [kg] is the weight of the measured body,  $g = 9.8066$  [m s<sup>-2</sup>] is the acceleration of gravity,  $r$  [m] is the pitch circle radius,  $T$  [s] is the period time,  $J_1$  [kg m<sup>2</sup>] is the inertia moment of plate hanger,  $l$  [m] is the cords length.

Calculated values of inertia moment of subframe (SUB) in Hypermesh compared with real measurement are shown in Table 3. Highest difference was found for inertia moment  $I_{yy}$  of 7.9%.

##### 5.2. EXPERIMENTAL MEASUREMENT

To validate dependencies of the elasto-kinematic parameters of the suspension obtained from simulations,

Subframe	$I_{xx}$ [kg m <sup>2</sup> ]	$I_{yy}$ [kg m <sup>2</sup> ]	$I_{zz}$ [kg m <sup>2</sup> ]
Computation	1.186	0.239	1.386
Measurement	1.221	0.258	1.432

TABLE 3. 3 Moments of inertia of subframe.

the experimental measurements on the vehicle using a test bench Beissbarth 1995 + VAS5080 were carried out. This device is designed to measure the geometrical parameters of suspension. The parameters, like the toe angle  $\delta$  and camber angle  $\gamma$ , depending on the vertical movement of the wheel  $D_z$ , were measured. The vehicle is established on the base plate of measuring stations. Wheel suspension stands on sliding supports (335 × 280 mm), allowing the wheels side-shift (change of axles track). Changing  $\Delta D_z$  enables to improve measurement accuracy. Measuring heads were installed on the rims, joined via linkage and established horizontally. Each head has two CDD cameras which transmit infrared light beam to measure geometric parameters of the wheel. Measurement configuration is shown in Figure 10.

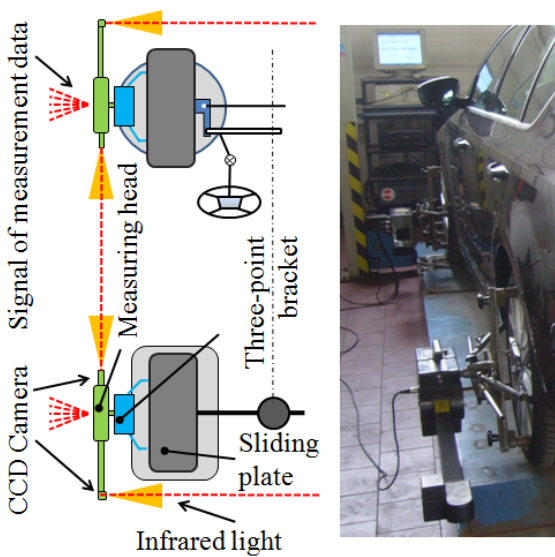


FIGURE 10. Configuration of the experimental measurement on the left side of the vehicle at Beissbarth testing device.

The measured vehicle is encumbered and unencumbered in order to move with the center of the wheel by a step of  $\Delta D_z = 10$  mm with the interval  $D_z = \langle -105, 105 \rangle$  mm, that is limited by the upper and lower stop. Measured values of  $\delta = f(D_z)$  and  $\gamma = f(D_z)$  are used for the comparison with the simulation results.

## 6. RESULTS AND DISCUSSION

Simulation results for individual variants of MBS computational model are geometrical parameters of axle suspension under the action of force load, as it is shown in Figure 8. Further outputs are the graphical maps

of the distribution of stresses and deformations of the examined supporting elements (Figure 1) which can be used during design, construction and optimization.

### 6.1. EFFECT OF SUPPORTING ELEMENTS FLEXIBILITY DURING WHEEL VERTICAL MOTION

Calculated dependencies of toe angle  $\delta = f(D_z)$  and the camber angle  $\gamma = f(D_z)$  for vertical movement of the wheel  $D_z$  for the individual variants of computational model are shown in Figure 11 and Figure 12.

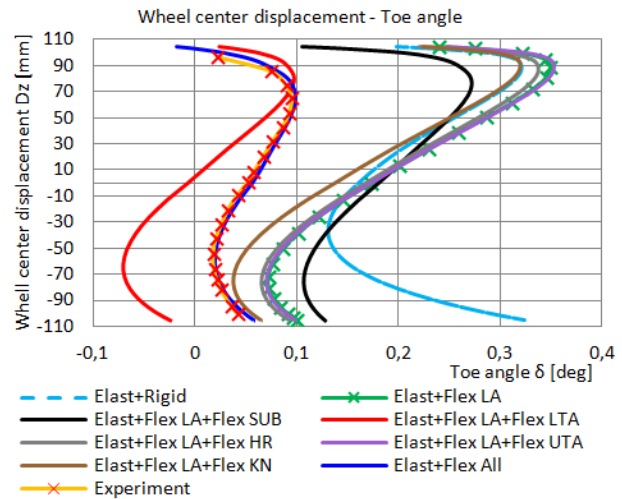


FIGURE 11. Dependence of  $\delta = f(D_z)$  for suspension with flexible supporting elements.

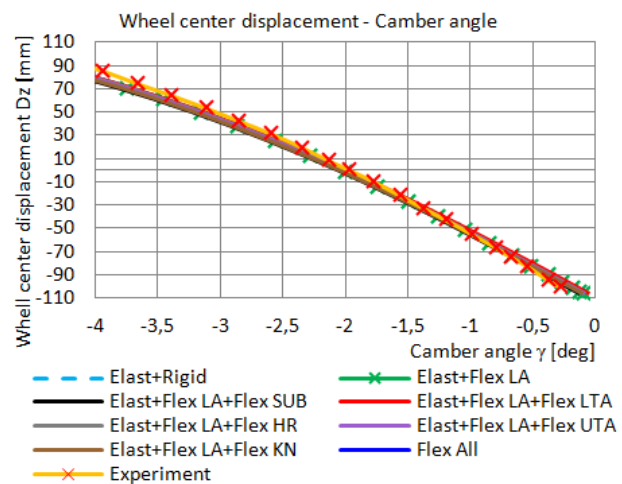


FIGURE 12. Dependence of  $\gamma = f(D_z)$  for suspension with flexible supporting elements.

They represent the main characteristics of elastokinematic properties of the suspension. Toe shape resembles an inverted letter S with the linear region in an interval around  $D_z = 0$  mm. From calculated values, it is evident that the flexibility of supporting elements in MBS models (Elast+Flex) strongly affects the value and shape of the toe angle  $\delta = f(D_z)$  and vary from the model with rigid elements (Elast+Rigid). Each element influences the course in another way. The

basic model Elast+Flex LA with flexible longitudinal arms differs most in the lower stop for  $D_z = -70$  mm, up to 139% compared to the model Elast-Rigid. Flexibility of the arm UTA and HR affects the toe angle  $\delta$  very slightly and shows the same behaviour as the model Elast+Flex LA. Flexibility of knuckle (KN) and LTA arm moves at the limit  $D_z = 0$ , the toe angle to  $\delta = 0.04^\circ$  and  $\delta = 0.18^\circ$  towards lower values. Subframe flexibility causes slope of the toe in linear segment. The tangent is 0.71 compared to the value of 0.48, which was found for the model Elast+Rigid with absolutely rigid supporting elements. Complex flexible model Elast+Flex All shows the movement of toe 0.12 deg towards lower values and the steepest linear section of the directive 1.21. Different courses of the toe angle for models in Figure 11 are caused by the flexibility of the supporting elements. The analysis shows that each suspension element affects the course  $\delta = f(D_z)$  differently.

The camber angle, on the other hand, does not differ for individual variants. Calculated values coincide very well with experimental measurements.

**6.2. EFFECT OF SUPPORTING ELEMENTS FLEXIBILITY DURING ACTION OF SIDE FORCE**

Elasto-kinematic properties of suspension with flexible supporting elements during action of side force  $FL$  show parameters  $\delta = f(FL)$  in Figure 13 and camber  $\gamma = f(FL)$  in Figure 14.

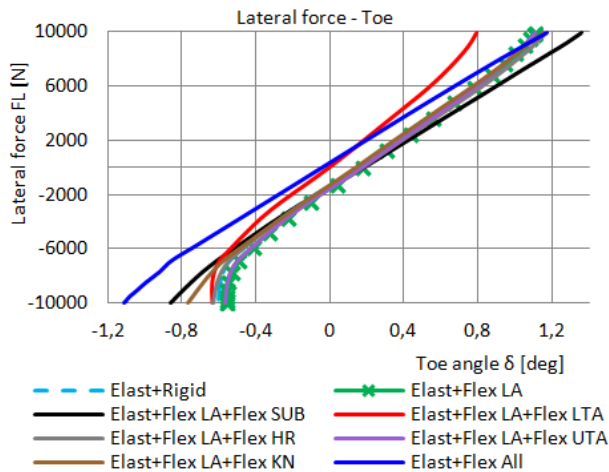


FIGURE 13. Dependence of  $\delta = f(FL)$  for suspension with flexible supporting elements.

Toe angle  $\delta$ , with decreasing longitudinal force  $FL$ , decreases linearly up to the border  $FL \sim -6850$  N, then it starts progression due to the nonlinear characteristics of bushings. The model taking into account arm flexibility LTA and model Elast Flex All differ from the model Elast+Rigid. Parameter  $FL = 0$  is shifted by  $\delta = 0.18^\circ$  and  $\delta = 0.12^\circ$  towards the lower values. The different values of the toe as well as for  $\delta = f(D_z)$  are caused by the flexibility of particular suspension elements.

The camber angle  $\gamma$  after a few sharp breaks in the value of  $FL = -6480$  N linearly decreases (negative values indicate negative camber). As it turns out, the biggest changes in camber are made by flexibility of the subframe and the knuckle. During the action of force  $FL = 4800$  N, formed by the rigid model of Elast+Rigid, the camber angle is  $\gamma = -1.29^\circ$ . For the flexible model Elast+Flex All it is  $\gamma = -0.87^\circ$ .

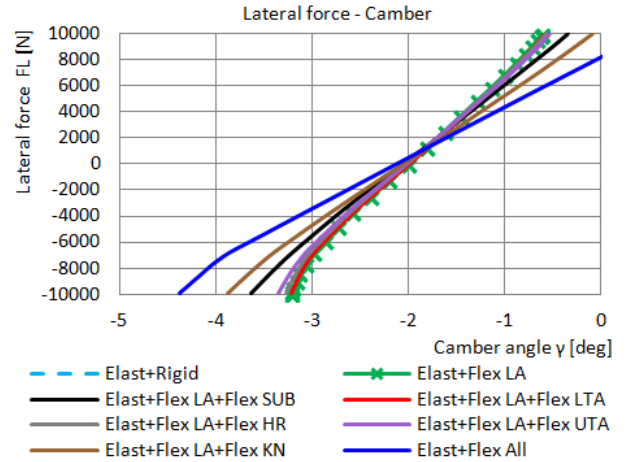


FIGURE 14. Dependence of  $\delta = f(FL)$  for suspension with flexible supporting elements.

Figure 15 shows the comparison of calculated variations with flexible bodies, in terms of changes in the geometric parameters of the linear section relative to the load change in  $\Delta FL = 1$  kN. The greatest variation of camber can be seen during the effect of the lateral force on the Elast+Flex All model  $\Delta\gamma = 0.257^\circ/1$  kN which is a difference of 70.2%, when compared to the rigid model. The highest change in the toe angle  $\Delta\delta = 0.119^\circ/1$  kN occurs in the model taking into account the compliance of subframe.

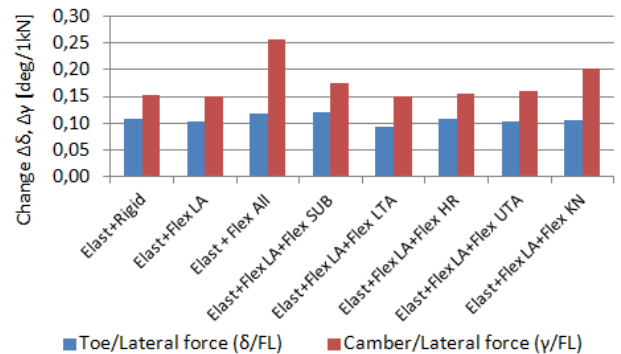


FIGURE 15. Change of toe angle  $\delta$  and camber  $\gamma$  during action of  $FL$  force.

**6.3. EFFECT OF SUPPORTING ELEMENTS FLEXIBILITY DURING ACTION OF LONGITUDINAL FORCE**

Calculated dependences of  $\delta = f(FB)$  in Figure 16 and  $\gamma = f(FB)$  in Figure 17 show the elasto-kinematic characteristics of the suspension under the action of

the longitudinal braking force  $FB$ . Toe angle  $\delta$  increases to approximately  $FB < 1\,225\text{ N}$ , after this break, it continues into linearly decreases. Models with flexible arms LA, UTA, HR and knuckle (KN) have the same characteristics like the model with rigid components. LTA model and fully flexible model Elast+Flex All show for  $FB = 4\,800\text{ N}$  the toe angle  $\delta = -0.149^\circ$  and  $\delta = -0.292^\circ$  compared to the rigid model with  $\delta = 0.111^\circ$ . Taking into account the flexibility of supporting elements thus generates considerable deviation from the rigid model.

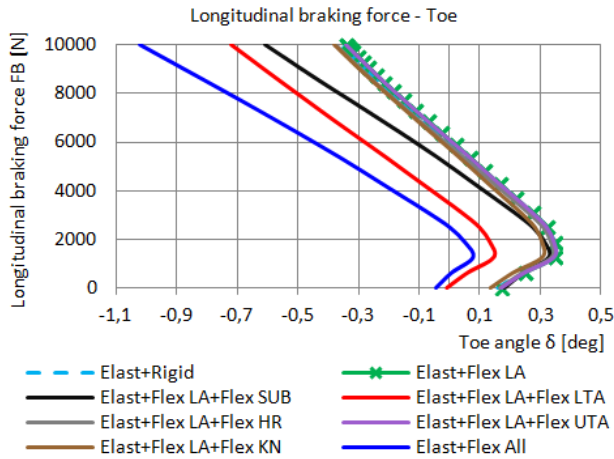


FIGURE 16. Dependence of  $\delta = f(FB)$  for models with flexible supporting elements.

Camber angle  $\gamma$  drops within the boundaries  $FB = 1\,225\text{ N}$  and for  $FB > 1\,225\text{ N}$  for all the studied variants except Elast+Flex All increases linearly. On the contrary, if we look at the model that takes into account the compliance of all the elements,  $N$  is linearly gradually decreasing in the interval of  $FB \in (1\,225, 10\,000)\text{ N}$ .

Consideration of knuckle flexibility in the model Elast+Flex LA+Flex KN causes another characteristics compared to the models with flexible arms and Elast+Rigid model. The highest variation during the exposure of the force  $FB = 4\,800\text{ N}$  compared to the rigid model ( $\gamma = -2.06^\circ$ ) was found for the model with the subframe flexibility ( $\gamma = -2.13^\circ$ ).

Different values of the toe angle and camber angle for  $FB = 0\text{ N}$  are caused by a static vertical load, which is determined by the weight of the vehicle.

Elasto-kinematic change of geometric parameters during exposure of longitudinal force  $FB$  is shown in Figure 18. During this load, the highest change in the toe  $\Delta\delta = -0.128^\circ/1\text{ kN}$  was found for the model Elast+Flex All, which is characterized by the lowest change of camber angle  $\Delta\gamma = 0.003^\circ/1\text{ kN}$ . The highest change in camber  $\Delta\gamma = 0.025^\circ/1\text{ kN}$  was found for the model Elast+Flex LA+Flex SUB, which contains the subframe flexible model.

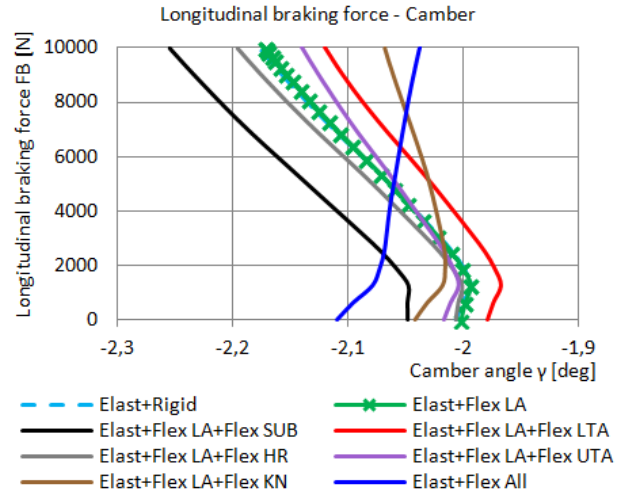


FIGURE 17. Dependence of  $\gamma = f(FB)$  for models with flexible supporting elements.

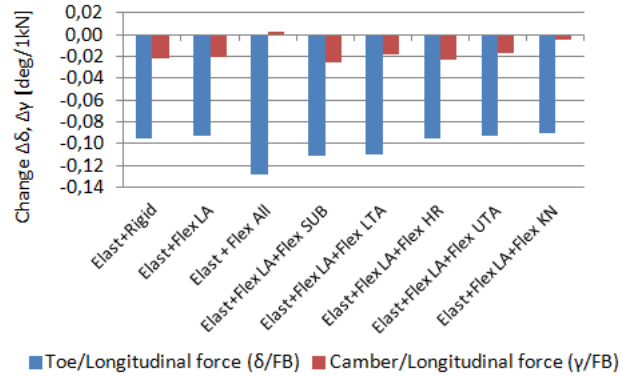


FIGURE 18. Changes of the toe angle  $\delta$  and camber angle  $\gamma$  during an action of longitudinal force  $FL$ .

## 7. CONCLUSION

This paper deals with the construction of the MBS computational model of an independent suspension, in which the flexibility of rubber-metal bushings, but also the flexibility of supporting elements (subframe, knuckle, longitudinal and transverse arms), are implemented. The model is then used to analyse the impact of these elements' flexibility on elasto-kinematic characteristics. Flexible FEM models discretized to 136 103 elements were created by Component Mode Synthesis by Craig-Bampton method and linked to the MBS model using RBE2-Spiders. The simulations show the impact of the flexibility of supporting elements on elasto-kinematic properties. It was shown that implementation of flexibility of the individual components strongly influences waveforms of geometrical parameters and final results significantly differ from the rigid model. The experimental measurement corresponds well with the model Elast+Flex All, which includes flexible models of all supporting elements. This model shows the highest changes in geometric parameters during the load. Significant changes can also be observed in case of the model Elast+Flex LA+Flex SUB reflecting the subframe

flexibility. During calculations of elasto-kinematic characteristics of suspension, it is very useful to take into account the flexibility of supporting elements. Thus it is possible to achieve the required accuracy of results.

## REFERENCES

- [1] M. Mitschke, H. Wallentowitz. *Dynamik der Kraftfahrzeuge*. Springer Fachmedien Wiesbaden, 2014. DOI:10.1007/978-3-658-05068-9.
- [2] K. Popp, W. Schiehlen. *Ground Vehicle Dynamics*. Springer Berlin Heidelberg, 2010. DOI:10.1007/978-3-540-68553-1.
- [3] C. Mousseau, T. Laursen, M. Lidberg, R. Taylor. Vehicle dynamics simulations with coupled multibody and finite element models. *Finite Elements in Analysis and Design* **31**(4):295–315, 1999. DOI:10.1016/S0168-874X(98)00070-5.
- [4] V. Stejskal, M. Valášek. *Kinematics and Dynamics of Machinery*. Marcel Dekker, New York, 1996.
- [5] D. Schramm, M. Hiller, R. Bardini. *Modellbildung und Simulation der Dynamik von Kraftfahrzeugen*. Springer Berlin Heidelberg, 2010. DOI:10.1007/978-3-540-89315-8.
- [6] J. Knapczyk, M. Maniowski. Elastokinematic modeling and study of five-rod suspension with subframe. *Mechanism and Machine Theory* **41**(9):1031–1047, 2006. DOI:10.1016/j.mechmachtheory.2005.11.003.
- [7] J. Knapczyk, S. Dzierzek. Displacement and force analysis of five-rod suspension with flexible joints. *Journal of Mechanical Design* **117**(4):532–538, 1995. DOI:10.1115/1.2826715.
- [8] T. Vrána, J. Bradáč, J. Kovanda. Study of wheel geometrical parameters for single-axle suspension by using elasto-kinematic model. In V. Adánek, M. Zajíček, A. Jonášová (eds.), *Computational mechanics 2015: 31st conference with international participation: Špičák, Czech Republic, November 9-11, 2015*, pp. 127–128. 2015.
- [9] P. Vokál. *Kinematika a dynamika zavěšení přední nápravy typu McPherson s uvažováním poddajnosti*. Ph.D. thesis, ČVUT v Praze, 1996.
- [10] J. Sajdl. *Elastokinematický model přední nápravy a metody jeho verifikace*. Ph.D. thesis, ČVUT v Praze, 2009.
- [11] L. Heuze, P. Ray, G. Gogu, et al. Design studies for a new suspension mechanism. In *Proceedings of the Institution of Mechanical Engineers*, vol. 217, pp. 529–535. 2003. DOI:10.1243/095440703322114915.
- [12] M. Goelke. *Practical Aspects of Multi-Body Simulation with HyperWorks*. Altair University, Michigan, 2015. Available on: <http://www.altairuniversity.com/14225-practical-aspects-of-multi-body-simulation-with-hyperworks-free-book/>.
- [13] J.-C.Samin, P.Fisette. *Symbolic Modeling of Multibody System*. Springer Netherlands, 2003. DOI:10.1007/978-94-017-0287-4.
- [14] V. Stejskal, J. Brousil, S.Stejskal. *Mechanika III*. ČVUT v Praze, 1993.
- [15] *MotionSolve Reference Guide 11.0*. Altair Engineering, Michigan, 2011. Available on: <http://www.altairhyperworks.com/ClientCenterHWTutorialDownload.aspx>.
- [16] J.-C.Samin, P.Fisette. *Multibody Dynamics: Computational methods and Application*. Springer Netherlands, 2013. DOI:10.1007/978-94-007-5404-1.